Development and Validation of a Model for Centrifugal Compressors in Reversed Flow Regimes

Katherine H. Powers *
Dept. of Mathematical Sciences
University of Bath
Claverton Down, Bath, BA2 7AY
United Kingdom
Email: k.h.powers@bath.ac.uk

Ian J. Kennedy
Dept. of Mechanical Engineering
University of Bath
Claverton Down, Bath, BA2 7AY
United Kingdom

Chris J. Brace
Dept. of Mechanical Engineering
University of Bath
Claverton Down, Bath, BA2 7AY
United Kingdom
Email: c.j.brace@bath.ac.uk

Paul A. Milewski
Dept. of Mathematical Sciences
University of Bath
Claverton Down, Bath, BA2 7AY
United Kingdom
Email: p.a.milewski@bath.ac.uk

Colin D. Copeland
School of Sustainable Energy Engineering
Simon Fraser University
University Drive, Surrey, V3T 0N1
BC, Canada
Email: colin_copeland@sfu.ca

ABSTRACT

Turbochargers are widely used to help reduce the environmental impact of automotive engines. However, a limiting factor for turbochargers is compressor surge. Surge is an instability that induces pressure and flow oscillations that often damages the turbocharger and its installation.

Most predictions of the surge limit are based on low-order models, such as the Moore-Greitzer model. These models tend to rely on a characteristic curve for the compressor created by extrapolating the constant speed lines of a steady-state compressor map into the negative mass flow region. However, there is little validation of these assumptions in the public literature.

*Please address all correspondence to this author.

In this paper, we develop further the first-principles model for a compressor characteristic presented in Powers, K., Brace, C., Budd, C., Copeland, C., & Milewski, P. (Aug 2020) "Modeling Axisymmetric Centrifugal Compressor Characteristics From First Principles." Journal of Turbomachinery 142(9), with a particular emphasis on reverse flow. We then perform experiments using a 58mm diameter centrifugal compressor provided by Cummins Turbo Technologies, where we feed air in the reverse direction though the compressor while the impeller is spinning in the forwards direction in order to obtain data in the negative mass flow region of the compressor map.

This demonstrated experimentally that there is a stable operating region in the reverse flow regime. The recorded data showed a good match with the theoretical model developed in this paper. We also identified a change in characteristic behaviour as the impeller speed is increased which, to the authors knowledge, has not been observed in any previously published experimental work..

INTRODUCTION

Turbochargers are components that use energy from engine exhaust gases to compress air prior to entering the engine. Using compressed air means there is more oxygen per unit volume in the engine cylinders, so more fuel can be burnt to increase the power output of that size of engine. Often turbochargers are used in combination with a downsized engine because smaller engines are more environmentally friendly. [1, 2]

With increasingly strict emissions regulations, the performance and efficiency of turbochargers is becoming a primary concern for manufacturers. For automotive turbochargers to perform effectively, they require a wide range of mass flows in which they can operate stably. However, this range is limited by compressor surge at low mass flows.

During operation at low mass flow rates, it is possible for a system level flow reversal to occur. When this happens, the average flow reverses direction and travels from the high pressure region at the compressor outlet to the low pressure region at the inlet. This flow reversal results in a drop in pressure at the compressor outlet, and so creates a condition that allows the flow to travel in the forward direction again. This oscillation in mass flow and pressure is termed surge [2]. Surge is an aerodynamic instability that is not only loud and off-putting to drivers, but is often damaging to the compressor and its installation.

Map based models are a popular method for predicting surge. These models use a function to describe the steady state behaviour of a compressor, usually from extending a compressor map beyond the surge

point into negative mass flows. There are many examples of these in the literature [3–8].

The majority of map-based models are based on a model by Greitzer [9] and Moore [10]. Here, a the model was derived by studying compression system consisting of a compressor and throttle valve separated by a pipe and large plenum. The Moore-Greitzer model [9–11] can be written as a system of ODEs to represent the pressure and mass flow in the pipework between the compressor and the throttle:

$$\frac{d\Phi}{dt} = B(\psi_c - \Psi) \tag{1}$$

$$\frac{d\Psi}{dt} = \frac{1}{B}(\Phi - \psi_T^{-1}) \tag{2}$$

where Φ and Ψ are the nondimensional mass flow and pressure respectively. The term ψ_T represents the pressure drop over the throttle. Typically the orifice equation

$$\psi_T = \xi_{T0} + \frac{1}{\xi_T^2}\Phi^2, \tag{3}$$

[11] is used.

The term ψ_c is the compressor characteristic, which represents the pressure rise over the compressor in steady-state conditions. This characteristic is difficult to determine. Koff and Greitzer [12] performed an experimental study on an axial compressor to determine its shape. They discovered that it was approximately cubic, so Moore and Greitzer [10] proposed using a cubic polynomial with parameters that can be fitted to compressor map data, i.e.

$$\psi_c = \psi_{c_0} + H\left[1 + \frac{2}{3}\left(\frac{\Phi}{W} - 1\right) - \frac{1}{2}\left(\frac{\Phi}{W} - 1\right)^3\right] \tag{4}$$

for parameters ψ_{c_0}, H and W. In 2008, Galindo et al. [13] did a similar experimental study for a small centrifugal compressor, also producing a cubic-like curve.

Since the compressor map data is contained within the positive mass flow region, using a cubic effectively extrapolates the trend into the negative flow region, meaning error can easily be induced here.

There have been some more theoretical approaches to determine the compressor characteristic. The

majority of those seen in the literature have involved mean-line or lumped parameter modelling, e.g. [14–16], but recently Powers et al. [17] developed a model from first principles. However, there is little evidence to validate these compressor characteristics in the reverse flow regime.

The reverse flow region is important because it contributes to the behaviour of the flow during deep surge cycles. Therefore, understanding the physics in the reversed flow region better could help us understand the nature of surge cycles and help mitigate their damaging behaviour.

Also, a more accurate representation of reverse flow will improve the accuracy of surge models. Surge models are vital for turbocharger and engine designers because they need to understand the operating regimes of the turbocharger and, more specifically, the limits in which they can operate safely.

The aim of this paper is to perform a more detailed study into the reversed flow region of the compressor characteristic. Firstly, we will further develop the model presented by Powers et al. [17], taking more care over the reversed flow region. Then we will perform experiments using a 58mm compressor in order to map this region and look at how the characteristic shape changes over different operating regimes. Finally, we will compare the experimental results to physical models for compressor characteristics, focusing in particular on the model developed here.

MATHEMATICAL MODEL

Powers et al. [17] developed a model for the compressor characteristics starting from the fundamental equations for conservation of mass, momentum (in a rotating frame) and energy:

$$\frac{\partial \rho}{\partial t} + \nabla \cdot (\rho \mathbf{u}) = 0, \tag{5}$$

$$\frac{\partial}{\partial t}(\rho \mathbf{u}) + \nabla \cdot (\rho(\mathbf{u} \otimes \mathbf{u})) + 2\rho(\mathbf{\Omega} \times \mathbf{u}) + \rho(\mathbf{\Omega} \times (\mathbf{\Omega} \times \mathbf{r})) = \rho \mathbf{g} - \nabla p + \nabla \cdot \tau, \tag{6}$$

$$\frac{\partial}{\partial t}(\rho E) + \nabla \cdot (\rho \mathbf{u} E + p\mathbf{u}) - \nabla \cdot (\tau \cdot \mathbf{u}) = \rho \dot{Q} \tag{7}$$

respectively, along with the ideal gas law $p = \rho R T$ and the assumption of a perfect gas (so the specific heat ratio, γ, is assumed constant).

This was reduced to a system of 1D ODEs in the radial direction by assuming:

(i) radial impeller blades, so $u_\theta = 0$ in the rotating frame, and

(ii) a vaneless diffuser with axisymmetric flow, so $\frac{\partial}{\partial \theta} = 0$,

and then averaging over the axial direction.

The resulting ODEs for the impeller were

$$\frac{1}{r}\frac{\partial}{\partial r}(rh\rho u_r) = 0, \tag{8}$$

$$\frac{1}{r}\frac{\partial}{\partial r}(rh\rho u_r^2) - h\rho\Omega^2 r = -h\frac{\partial p}{\partial r} + hF_r, \tag{9}$$

$$\frac{1}{r}\frac{\partial}{\partial r}\left(rh\rho u_r\left(\frac{u_r^2}{2} + \frac{\gamma}{\gamma-1}\frac{p}{\rho} - \frac{\Omega^2 r^2}{2}\right)\right) = 0, \tag{10}$$

and for the diffuser were

$$\frac{1}{r}\frac{\partial}{\partial r}(rh\rho u_r) = 0, \tag{11}$$

$$\frac{1}{r}\frac{\partial}{\partial r}(rh\rho u_r^2) - \frac{h\rho u_\theta^2}{r} = -h\frac{\partial p}{\partial r} + hF_r, \tag{12}$$

$$\frac{1}{r}\frac{\partial}{\partial r}(rh\rho u_r u_\theta) + \frac{h\rho u_r u_\theta}{r} = hF_\theta, \tag{13}$$

$$\frac{1}{r}\frac{\partial}{\partial r}\left(rh\rho u_r\left(\frac{u_r^2}{2} + \frac{u_\theta^2}{2} + \frac{\gamma}{\gamma-1}\frac{p}{\rho}\right)\right) = 0, \tag{14}$$

where

$$F_r = \frac{f}{2}\rho u_r^2 S \tag{15}$$

$$F_\theta = \frac{f}{2}\rho u_r u_\theta S \tag{16}$$

represent skin friction.

A relationship for the friction parameter was found from performing a least squares fit to data:

$$f = 0.14 + 5 \times 10^{-6}\Omega. \tag{17}$$

This was validated against different compressor geometries to show its potential as a universal relationship.

Powers et al. [17] also created a stall function to take into account how the compressor responds to

incidence losses and any resulting local recirculation. We have deviated from their work and propose a new stall function, ξ.

Writing

$$\dot{m} = \xi A \rho u_r, \tag{18}$$

we see that ξA represents the area of the channel that is not blocked due to stall. Therefore, at $\xi = 1$ the flow is not stalled and at $\xi = 0$ the flow is completely stalled.

We shall assume that, like Powers et al., when the flow stalls, the velocity is continuous with a continuous gradient. However, instead of forcing the unstalled flow velocity to be zero at zero mass flow, we shall assume that the velocity of the unstalled flow increases with stalling and will be a maximum when the system is fully stalled.

It may sound counter-intuitive to allow a non-zero velocity for the unstalled portion of the flow when the average flow is zero. However, let subscripts u and s denote unstalled and stalled portions respectively, then

$$\dot{m} = A_s \rho \cancelto{0}{u_s} + \cancelto{0}{A_u} \rho u_u = 0. \tag{19}$$

This shows us that at $\dot{m} = 0$, all of the flow is stalled and so have an average velocity of zero, and none of the flow is unstalled so it is a valid to have a non-zero velocity at that point.

These assumptions result in

$$\xi = \frac{1}{\frac{1}{2}\left(\frac{\tan\beta_B}{\tan\beta} + \frac{\tan\beta}{\tan\beta_B}\right) + \hat{a}\left(1 + \frac{1}{2}\frac{\tan\beta}{\tan\beta_B}\right)\left(\frac{\tan\beta_B}{\tan\beta} - 1\right)^2}, \tag{20}$$

where $\hat{a}$ is the parameter that controls the level of stalling (see Appendix A for full derivation).

Since this is a different function to the stall parameter from Powers et al. we cannot use their correlation. Surge tests were performed using the same turbocharger as in the reverse flow tests below. Using the amplitude of the pressure oscillations during a deep surge cycle, we determined that $\hat{a} = 1.7$ for this

compressor (see Fig. 1). Unlike Powers et al. this is not a universal relation and so further work is needed to develop a relationship for the stall parameter so the model developed can remain predictive.

The stall function created by Powers et al. [17] had a local minimum in the positive flow region, which implied that the flow would recover from surge and be stable at a low enough forward mass flow. However, this new function effectively shifts the local minimum in the characteristic so that it is at zero mass flow, meaning that, once the flow is surging, it will continue to surge as the mass flow is reduced to zero, and only once the flow is reversed will it stabilise.

Reverse flow

We shall now make a few small changes to this model to make it suitable for the reverse flow case. First, it is important to note that Powers et al. [17] changed the sign of the friction parameter for negative mass flows, even though this wasn't explicitly stated, because friction will always oppose motion. Therefore, for reverse flow the ODEs are

$$\frac{1}{r}\frac{\partial}{\partial r}(rh\rho u_r) = 0 \tag{21}$$

$$\frac{1}{r}\frac{\partial}{\partial r}(rh\rho u_r^2) - h\rho\Omega^2 r = -h\frac{\partial p}{\partial r} + hf\rho u_r^2\left(\frac{1}{h} + \frac{n_b}{2\pi r}\right) \tag{22}$$

$$\frac{1}{r}\frac{\partial}{\partial r}\left(rh\rho u_r\left(\frac{u_r^2}{2} + \frac{\gamma}{\gamma-1}\frac{p}{\rho} - \frac{\Omega^2 r^2}{2}\right)\right) = 0 \tag{23}$$

for the impeller and

$$\frac{1}{r}\frac{\partial}{\partial r}(rh\rho u_r) = 0 \tag{24}$$

$$\frac{1}{r}\frac{\partial}{\partial r}(rh\rho u_r^2) - \frac{h\rho u_\theta^2}{r} = -h\frac{\partial p}{\partial r} + h\frac{f}{h}\rho u_r^2 \tag{25}$$

$$\frac{1}{r}\frac{\partial}{\partial r}(rh\rho u_r u_\theta) + \frac{h\rho u_r u_\theta}{r} = h\frac{f}{h}u_r u_\theta \tag{26}$$

$$\frac{1}{r}\frac{\partial}{\partial r}\left(rh\rho u_r\left(\frac{u_r^2}{2} + \frac{u_\theta^2}{2} + \frac{\gamma}{\gamma-1}\frac{p}{\rho}\right)\right) = 0 \tag{27}$$

for the diffuser.

The main changes we suggest are related to the boundary conditions. Powers et al. used the same conditions as forward flow, i.e. having a known mass flow, ambient pressure, and ambient density at the

impeller inlet, but these will be unrealistic for the reversed flow regime.

In reality, the density of the air exiting the impeller inlet need not be the same as ambient air. Instead we can use the condition that the temperature of the air being fed into the compressor (i.e. at the diffuser outlet) is constant. This now means we have to solve a boundary value problem, which can be done via the shooting method.

Another condition we need to provide is the value for the tangential velocity entering the diffuser, $u_{\theta D}$. The absolute velocity in the volute is given by

$$u = \sqrt{u_r^2 + u_\theta^2}. \tag{28}$$

In forward flow, the volute is designed purely to collect the air around the diffuser. The area increase in the volute is to account for the increase in mass being added to the volute as this happens, therefore the properties of the gas in the volute, e.g. velocity and density, are reasonably constant. Therefore, it seems reasonable to assume that the velocity and density are unchanged in the volute in reverse flow conditions too, and so $\rho =$ const. and

$$u = \sqrt{u_{rD}^2 + u_{\theta D}^2}. \tag{29}$$

We know that, from Eqn. 24, the mass flow at the outermost radius of the diffuser is given by

$$\dot{m} = 2\pi r_D h_D \rho u_{rD} = A_D \rho u_{rD}. \tag{30}$$

We also know at the critical area of the volute, A^*, all of the mass has been collected and will pass through this area with velocity u. Therefore,

$$\dot{m} = A^* \rho u. \tag{31}$$

Equating these gives us

$$u = \frac{A_D}{A^*} u_{rD} \tag{32}$$

$$\implies u_{rD}^2 + u_{\theta D}^2 = \left(\frac{A_D}{A^*}\right)^2 u_{rD}^2 \tag{33}$$

$$\implies u_{\theta D}^2 = \left[\left(\frac{A_D}{A^*}\right)^2 - 1\right] u_{rD}^2 \tag{34}$$

$$\implies u_{\theta D} = u_{rD}\sqrt{\left(\frac{A_D}{A^*}\right)^2 - 1}. \tag{35}$$

For the geometry of the compressor used for testing in the following sections, this gives us a flow angle into the diffuser from the volute of

$$\theta = \tan^{-1}\left(\frac{u_{\theta D}}{u_{rD}}\right) = \tan^{-1}\left(\sqrt{\left(\frac{A_D}{A^*}\right)^2 - 1}\right) = 39.3^o. \tag{36}$$

However, it is interesting to note that the resulting pressure simulated in the reverse flow case is not very sensitive to this angle. Changing the angle between 20^o to 60^o resulted in a maximum difference of 5%.

The final change we suggest is the need to account for shear losses as we go from the diffuser to the impeller. We are considering flow reversal in the situation where the impeller still rotates in the conventional direction but the air is travelling from the volute backwards through the compressor (see Fig. 2(a)). This will result in a shear layer at the impeller-diffuser interface because of a huge change in tangential velocity. The air not only changes direction but is accelerated to the large rotational speed of the impeller in a very short radial distance. This will result in a large amount of viscous dissipation, which was considered small and so neglected during the derivation of the ODEs for the impeller and diffuser.

To see what happens over this shear layer, let's consider the impeller-diffuser interface in the x-y coordinate system shown in Fig. 2(b). In this case, we can assume that all variables are independent of x. This

means that conservation of mass, momentum and energy become

$$(\rho v)_y = 0 \tag{37}$$

$$\rho v u_y = -p_x + \mu u_{yy} \tag{38}$$

$$\rho v v_y = -p_y + \mu v_{yy} \tag{39}$$

$$\rho v e_y = -p v_y + \lambda v_y^2 + \mu u_y^2 + 2\mu v_y^2 \tag{40}$$

respectively, where subscripts have been used to denote differentiation [18]. Let's assume that the flow across the shear layer is incompressible, so conservation of mass leads to $v_y = 0$. Then conservation of energy becomes

$$\rho v \frac{\partial e}{\partial y} = \mu \left(\frac{\partial u}{\partial y} \right)^2 \tag{41}$$

$$\implies \frac{\rho v}{\gamma - 1} \frac{\partial}{\partial y} \left(\frac{p}{\rho} \right) = \mu \left(\frac{\partial u}{\partial y} \right)^2 \tag{42}$$

$$\implies \frac{v}{\gamma - 1} \frac{\partial p}{\partial y} = \mu \left(\frac{\partial u}{\partial y} \right)^2 . \tag{43}$$

We can approximate these derivatives by assuming the shear layer has a thickness δ to give,

$$\frac{v}{\gamma - 1} \frac{\Delta p}{\delta} = \mu \left(\frac{\Delta u}{\delta} \right)^2 \tag{44}$$

$$\implies \Delta p = \frac{\mu(\gamma - 1)}{v \delta} (\Delta u)^2 . \tag{45}$$

Therefore, returning to previous notation we have a pressure jump of

$$p_I = p_D + \nu (u_{\theta I} - u_{\theta D})^2 , \tag{46}$$

at the impeller-diffuser interface, where

$$\nu = \frac{\mu(\gamma - 1)}{u_r \delta} \tag{47}$$

is our shear loss parameter.

For the model presented here, we will assume that the parameter ν is always finite. For this to be the case, $u_r \neq 0$ and so some form of transport always occurs across the impeller-diffuser interface. We believe this is a reasonable assumption because, due to turbulent flow, we would expect some flux across the boundary even when the average mass flow is zero. However, there is scope for further research into the form of this shear loss.

To determine ν we will assume that the width of the shear layer δ is such that there is continuity in static pressure at zero mass flow between the forward flow and reverse flow models. This tells us

$$\nu \propto u_\theta^2 \tag{48}$$

(see Fig. 3), which makes sense because it is likely that shear losses increase with the turbulent kinetic energy of the system.

All of the above modifications gives us the compressor characteristic shown in Fig. 4.

Quasi-steady model

These compressor characteristics can be used within quasi-steady models for surge. For example, Powers et al. [17] developed the following model:

$$\frac{d\dot{m}}{dt} = \frac{A}{L}(p_c(\dot{m}) - p) + \frac{\kappa^{\frac{1}{\gamma}}}{AL}\left(\frac{\dot{m}^2}{p_c(\dot{m})^{\frac{1}{\gamma}}} - \frac{\dot{m}_T(p)^2}{p^{\frac{1}{\gamma}}}\right), \tag{49}$$

$$\frac{dp}{dt} = \frac{\gamma\kappa^{\frac{1}{\gamma}}}{AL} p^{\frac{\gamma-1}{\gamma}}(\dot{m} - \dot{m}_T(p)), \tag{50}$$

where $\dot{m}_T$ is the throttle characteristic and p_c is the steady-state compressor characteristic.

It is important to understand that the compressor characteristic, though important, is not the only ingre-

dient needed to understand the surge phenomenon. We know that surge is a system level phenomenon and so depends on the geometry of the test rig pipework, but it is only here in the quasi-steady model that this comes into play. In this case, the terms A and L are the cross-sectional area and length of the pipework between the turbocharger and the throttle valve, but it is possible to adopt quasi-steady models that take into account inlet geometry as well.

PROCEDURE

To validate this model a turbocharger was tested using the gas stand facilities at the University of Bath. Table 1 gives the geometric details of the turbocharger compressor, where Fig. 5 can be used for reference.

In the facility, compressed air was supplied through two separate electrically heated flow paths. Gate valves were used to control the flow. One flow was used to drive the turbine and was in the conventional direction, entering at the turbine inlet. This was the predominant means of controlling the speed of the turbocharger. The other compressed air stream was fed in the reverse flow direction through the compressor, entering at the compressor outlet. See Fig. 6 for a schematic of the test rig set-up.

To run the experiment, air was let into the turbine side to drive the rotor. The valve feeding air to the compressor outlet remained closed so there was no air going through the compressor side. This led to surging behaviour with an audible pulsating flow. The turbine speed was limited to approximately 20,000 rpm so not to cause damage to the compressor.

Compressed air was then fed into the compressor side in the reverse direction by opening the valve. This stopped the surging behaviour and stabilised the flow.

The turbine speed was then increased to the desired values. The compressor side valve was adjusted to keep the flow in the stable backflow regime throughout the testing. At fixed speeds, the compressor side mass flow was slowly increased from 15g/s to 80g/s to map out the reversed flow characteristic. This was repeated multiple times and for multiple different speeds.

A high-frequency pressure measurement was recorded to check the steadiness of the flow. Since the flow was found to be steady, measurements were taken at 10Hz of the mass flow, temperature and pressure on the compressor side. A V-cone was used to measure the mass flow, PRTs for the temperature, and pneumatically averaged pressure transducers for static and total pressure measurements. The locations and accuracy of these measurements are indicated in Fig. 6.

RESULTS AND DISCUSSION

The first interesting observation was that the flow was surging when the valve feeding air into the compressor was fully closed. A snapshot of this is shown in Fig. 7. Therefore, it is highly probable that the flow dynamics are continually unsteady between zero flow and the surge line in forward flow. Combining this with the fact that the flow dynamics at negative mass flows was observed to be steady, shows us that a switch of stability has to occur at zero mass flow. Therefore, this supports our new stall function with a local minimum at zero flow.

The next important result to recognise is that the flow is steady in the reverse flow region. Consider the Moore-Greitzer model (Eqns. 1 & 2) [11]:

$$\frac{d\Phi}{dt} = B(\psi_c - \Psi) = f(\Phi, \Psi), \tag{51}$$

$$\frac{d\Psi}{dt} = \frac{1}{B}(\Phi - \psi_T^{-1}) = g(\Phi, \Psi). \tag{52}$$

Computing the Jacobian, J, allows us to determine regions of stability for this model:

$$J = \begin{bmatrix} \frac{df}{d\Phi} & \frac{df}{d\Psi} \\ \frac{dg}{d\Phi} & \frac{dg}{d\Psi} \end{bmatrix} = \begin{bmatrix} B\frac{d\psi_c}{d\Phi} & -B \\ \frac{1}{B} & -\frac{1}{B}\left(\frac{d\psi_T}{d\Phi}\right)^{-1} \end{bmatrix}. \tag{53}$$

The system is stable if $\det J > 0$ and tr$J < 0$ [19]. In our case,

$$\det J = 1 - \frac{d\psi_c}{d\Phi}\left(\frac{d\psi_T}{d\Phi}\right)^{-1}, \tag{54}$$

$$\text{tr}J = B\frac{d\psi_c}{d\Phi} - \frac{1}{B}\left(\frac{d\psi_T}{d\Phi}\right)^{-1}. \tag{55}$$

The surge models in literature all have a throttle characteristic with a positive gradient (see Fig. 4). Also, as most models are based on the cubic characteristic of Moore and Greitzer (Eqn. 4) they tend to assume a negative gradient of the compressor characteristic. The model we developed above also has this feature of a negative slope in the reverse flow region.

This means that

$$\frac{d\psi_T}{d\Phi} > 0 > \frac{d\psi_c}{d\Phi} \tag{56}$$

$$\implies \frac{d\psi_c}{d\Phi}\left(\frac{d\psi_T}{d\Phi}\right)^{-1} < 1 \tag{57}$$

$$\implies \det J > 0 \tag{58}$$

and

$$\frac{d\psi_T}{d\Phi} > 0, \frac{d\psi_c}{d\Phi} < 0 \tag{59}$$

$$\implies \mathrm{tr}J = B\frac{d\psi_c}{d\Phi} - \frac{1}{B}\left(\frac{d\psi_T}{d\Phi}\right)^{-1} < 0 \tag{60}$$

so having a negative gradient of the compressor characteristic results in a mathematically stable system and hence steady flow. So observing experimentally stable flow supports compressor characteristics having a negative gradient in the negative mass flow region.

Figure 8(a) shows the raw test data obtained in the pressure-mass flow plane at different impeller speeds. Figure 8(b) shows how this data compares to the model developed in the previous sections. We can see that we achieve a good quantitative fit to our model for all points, except the near-zero points at higher impeller speeds.

The 85krpm and 95krpm speed lines also have a good qualitative fit because they share the same quadratic-like shape that our model predicts. Therefore, the model we developed above must capture the predominant physics going on in reverse flow.

Looking closely at the raw data, we can see a gradual change in shape of the reverse flow characteristic as the impeller speed increases. We can see that, for 105krpm and 115krpm, the data points appear to be tending to a vertical asymptote close to zero flow. These possible asymptotes have been added in grey to Fig. 8(b). This is the first time something like this has been recorded in literature.

We note here that the V-cone used to measure the mass flow was within the measurement range but reaching the lower limit at which we would see ± 0.5% accuracy. However, the pressure sensor will still be accurate in this range so the characteristic shapes observed are valid with some possible variation in the

location of this vertical asymptote.

This asymptote suggests that, at high impeller speeds, there is a minimum reverse mass flow required to overcome the operation of the compressor in steady state. This is effectively a rotor head because pressure is created due to the rotation of the impeller. This rotor head will be larger for higher rotational speeds. This explains why the theoretical asymptote for 115krpm crosses 1bar pressure at a larger negative flow rate than 105krpm: a higher fluid momentum is required to overcome the rotor head.

It is possible that a different form of the shear loss to Eqns. 46-47 would allow the model to capture this asymptotic behaviour. For example, we assumed ν to be finite but relaxing this assumption would allow for the possibility of asymptotes developing near zero flow.

Having this vertical asymptote at near-zero mass flow would likely cause the deep surge cycles to have large pressure amplitudes since the trajectories of surge cycles tend to track the mathematically stable regions of the compressor characteristic closely (see e.g. [9, 11, 17]). Therefore, the trajectory tracking the reverse flow part of this observed compressor characteristic will include transient dynamics passing through near atmospheric pressure values, as shown in Fig. 9. This large amplitude pressure oscillation would explain why surge cycles can be far more violent at higher speeds than lower ones.

Being able to model this reverse flow phenomenon is really important because modelling is the first step in the management of a system. From there it might be possible to optimise the system to reduce the violence of deep surge cycles.

Figure 10(a) shows multiple runs overlayed for the 85krpm and 115 krpm speed lines, the temperature at each of these runs is shown in Fig. 10(b). These runs were performed on different days, with the test cell starting cold and starting warm. For low impeller speeds the repeatability was good. However, the variability in the repeats increased with impeller speed.

From looking at the plots of temperature, we believe that this is not the cause of the variability. There is a large variability in the temperature of the points at both speeds, but only minimal change in the repeat runs for 85krpm. If it were the temperature, we would expect to see the variability in both 85krpm and 115krpm.

During testing, we noticed that the main cause of variation seemed to be the starting condition. We usually started at low mass flows and swept gradually upwards to larger ones, but starting part way up this sweep gave us different results initially. This could mean that either (i) the system itself is sensitive, or (ii) the two types of dynamics creating the change in characteristic shape are interacting or can be observed at the same mass flow dependent on the starting conditions.

It is interesting to note that the highest temperatures recorded for 115krpm coincide with the points

at which we get this transition from the quadratic-like shape to the asymptotic behaviour. Therefore, any physical phenomenon that causes this transition appears to result in a large rise in temperature.

We tested two identical turbochargers during these reversed flow experiments and we have plotted the results from both on Fig. 10. There is standard manufacturing variability between the two turbochargers, but it is interesting to note that both turbochargers observed this change in characteristic shape with impeller speed.

We would have liked to obtain results at higher impeller speeds. However, pushing the turbine to higher speeds while maintaining the reversed flow conditions in the impeller leads to catastrophic failure of the turbocharger (see Fig. 11). We also decided not to test at larger negative mass flows due to the risk of causing a failure, because the temperature of the system was reaching values over 200^{o}C.

CONCLUSIONS

The majority of surge models for turbochargers rely on a steady-state compressor characteristic that is extrapolated into the reverse flow region. We have conducted experiments to measure the characteristic in the region of negative mass flows. We have shown that the flow operates stably in this case, which provides supporting evidence for the models like the Moore-Greizter model.

We further developed the model by Powers et al. [17], taking care of the dynamics and boundary conditions that hold in reversed flow conditions. We suggested a new stall function that results in a characteristic with a local minimum at zero flow, and have provided supporting experimental evidence for this.

We experimentally identified a change in characteristic shape as the impeller speed increases. This is the first time such a change has been recorded, and it suggests that the physical dynamics of the flow change at high impeller speeds at near-zero flow.

The model in the reverse flow regime showed excellent agreement to the experimental data. However, the model doesn't currently capture the change in characteristic shape. This phenomenon is likely to be caused by a rotor head, and further work is planned to incorporate this into the mathematical model by using a different form of shear loss at the impeller-diffuser interface.

ACKNOWLEDGEMENTS

The authors very are grateful to Cummins Turbo Technologies for their continued support of this work and, particularly, for providing the turbochargers used for carrying out this test work.

Katherine Powers is supported by a scholarship from the EPSRC Centre for Doctoral Training in Statis-

tical Applied Mathematics at Bath (SAMBa), under the project EP/L015684/1.

NOMENCLATURE

A Cross-sectional area

$\hat{a}$ Stalling factor

B Greitzer's parameter

$\det$ Determinant

E Specific energy

f Friction factor

F Skin friction

$\mathbf{g}$ Acceleration due to gravity

h Channel height

J Jacobian

L Length

$\dot{m}$ Mass flow

n_b Number of impeller blades

p Static pressure

$\dot{Q}$ Heat transfer

q Mass flow per radian

R Specific gas constant

S Surface area per unit volume

T Temperature

tr Trace

u Velocity

β Flow angle

β_B Blade angle

δ Thickness of shear layer

γ Specific heat ratio

κ Isentropic constant

λ Second viscosity coefficient

μ Dynamic viscosity

ν Parameter for shear loss

ξ Stall parameter

ξ_T Throttle parameter

ρ Density

τ Stress

Φ Nondimensional mass flow

Ψ Nondimensional pressure

Ω Angular velocity

Subscripts:

c Compressor

D Diffuser

I Impeller

r Radial direction

s Stalled flow

T Throttle

u Unstalled flow

x Differentiation w.r.t. x

y Differentiation w.r.t. y

θ Tangential direction

Abbreviations:

ODE Ordinary differential equation

REFERENCES

[1] Stone, R., 2012. *Introduction to internal combustion engines*, 4 ed. Palgrave MacMillan.

[2] Watson, N., and Janota, M. S., 1982. *Turbocharging: The internal combustion engine*. MacMillan.

[3] Emmons, H. W., Pearson, C. E., and Grant, H. P., 1955. "Compressor surge and stall propagation, traks". ASME.

[4] Fink, D. A., Cumpsty, N. A., and Greitzer, E. M., 1992. "Surge dynamics in a free-spool centrifugal compressor system". *Journal of Turbomachinery,* **114**, pp. 321– 332.

[5] Arnulfi, G. L., Giannattasio, P., Giusto, C., Massardo, A. F., Micheli, D., and Pinamonti, P., 1999. "Multistage centrifugal compressor surge analysis: Part II - Numerical simulation and dynamic control parameters evaluation". *Journal of Turbomachinery,* **121**(2), pp. 312–320.

[6] Van Helvoirt, J., de Jager, B., Steinbuch, M., and Smeulers, J., 2004. "Stability parameter identification for a centrifugal compression system". In Decision and Control, 2004. CDC. 43rd IEEE Conference on, Vol. 4, IEEE, pp. 3400–3405.

[7] Mizuki, S., Asaga, Y., Ono, Y., and Tsujita, H., 2006. "Investigation of surge behavior in a micro centrifugal compressor". *Journal of Thermal Science,* **15**(2), p. 97.

[8] Bozza, F., and De Bellis, V., 2011. "Map-based and 1d simulation of a turbocharger compressor in surging operation". *SAE International Journal of Engines,* **4**(2), pp. 2418–2433.

[9] Greitzer, E. M., 1976. "Surge and rotating stall in axial flow compressors - Part I: Theoretical compression system model". *Journal of Engineering for Power,* **98**(2), pp. 190–198.

[10] Moore, F. K., and Greitzer, E. M., 1986. "A theory of post-stall transients in axial compression systems: Part I - Development of equations". *Journal of Engineering for Gas Turbines and Power,* **108**(1), pp. 68–76.

[11] Hős, C., Champneys, A., and Kullmann, L., 2003. "Bifurcation analysis of surge and rotating stall in the Moore–Greitzer compression system". *IMA Journal of Applied Mathematics,* **68**(2), pp. 205–228.

[12] Koff, S. G., and Greitzer, E. M., 1984. "Stalled flow performance for axial compressors: I - Axisymmetric characteristic". In 29th International Gas Turbine Conference and Exhibit, Vol. 1, American Society of Mechanical Engineers.

[13] Galindo, J., Serrano, J., Climent, H., and Tiseira, A., 2008. "Experiments and modelling of surge in small centrifugal compressor for automotive engines". *Experimental Thermal and Fluid Science,* **32**(3), pp. 818–826.

[14] Japikse, D., 1996. *Centrifugal compressor design and performance*, Vol. 2. Concepts Eti White River Junction, VT.

[15] Martin, G., Talon, V., Higelin, P., Charlet, A., and Caillol, C., 2009. "Implementing turbomachinery physics into data map-based turbocharger models". *SAE International Journal of Engines,* **2**(1), pp. 211–229.

[16] Elder, R. L., and Gill, M. E., 1985. "A discussion of the factors affecting surge in centrifugal compressors". *Journal of Engineering for Gas Turbines and Power,* **107**, pp. 499–506.

[17] Powers, K. H., Brace, C. J., Budd, C. J., Copeland, C. D., and Milewski, P. A., 2020. "Modeling

axisymmetric centrifugal compressor characteristics from first principles". *Journal of Turbomachinery,* **142**(9).

[18] Currie, I. G., 2016. *Fundamental mechanics of fluids*. CRC press.

[19] Arrowsmith, D. K., and Place, C. M., 1990. *An introduction to dynamical systems*. Cambridge university press.

APPENDIX A: DERIVATION OF IMPELLER STALL FUNCTION

When impeller inlet stall occurs, we assume this causes a blockage within the channel (see Fig. 12). To represent this blockage we create a stall function, ξ, where $\dot{m} = \xi A \rho u_r$. This means that ξA represents the area of the channel that is not blocked due to the stall, and so is the area that is available for the flow to pass through.

If β is the angle of the flow entering the impeller, and β_B is the impeller inlet blade angle, then we assume stall occurs in the impeller only for $\beta > \beta_B$ and is smoothly increasing in severity until a maximum at zero flow. This implies that $\xi = 1$ when $\beta = \beta_B$ and $\xi = 0$ when $\dot{m} = 0$ (i.e. the entire channel is blocked due to stall, so the effective area is zero).

We can find the stall function by considering the velocity as a function of the mass flow, i.e. $u_r(\dot{m}) = \frac{\dot{m}}{\xi A \rho}$. For ξ to result in a smooth function, we assume that at $\beta = \beta_B$

$$u_r(\dot{m}_B) = \frac{\dot{m}_B}{A\rho}, \tag{A1}$$

$$\frac{du_r}{d\dot{m}}(\dot{m}_B) = \frac{1}{A\rho}. \tag{A2}$$

For the velocity to reach a maximum at zero flow, we get that

$$\frac{du_r}{d\dot{m}}(0) = 0. \tag{A3}$$

We desire a free parameter in the stall function in order to set the strength of this stall based on experimental data. Therefore, with three conditions and a free parameter, the simplest function we can use to describe the stalled velocity is a cubic:

$$u_r = a\dot{m}^3 + b\dot{m}^2 + c\dot{m} + d. \tag{A4}$$

Differentiating this gives

$$\frac{du_r}{d\dot{m}} = 3a\dot{m}^2 + 2b\dot{m} + c. \tag{A5}$$

Therefore, Eqn. A3 leads to $c = 0$ and Eqn. A2 gives us

$$3a\dot{m}_B^2 + 2b\dot{m}_B = \frac{1}{A\rho} \tag{A6}$$

$$\implies b = \frac{1}{2A\rho\dot{m}_B} - \frac{3}{2}a\dot{m}_B. \tag{A7}$$

Finally, Eqn. A1 gives us

$$a\dot{m}_B^3 + \left(\frac{1}{2A\rho\dot{m}_B} - \frac{3}{2}a\dot{m}_B\right)\dot{m}_B^2 + d = \frac{\dot{m}_B}{A\rho} \tag{A8}$$

$$\implies d = \frac{\dot{m}_B}{2A\rho} + \frac{a}{2}\dot{m}_B^3. \tag{A9}$$

Therefore, the stalled velocity has the form

$$u_r(\dot{m}) = a\dot{m}^3 + \left(\frac{1}{2A\rho\dot{m}_B} - \frac{3}{2}a\dot{m}_B\right)\dot{m}^2 + \left(\frac{\dot{m}_B}{2A\rho} + \frac{a}{2}\dot{m}_B^3\right) \tag{A10}$$

$$\implies \frac{\dot{m}}{A\rho\xi} = a\dot{m}^3 + \left(\frac{1}{2A\rho\dot{m}_B} - \frac{3}{2}a\dot{m}_B\right)\dot{m}^2 + \left(\frac{\dot{m}_B}{2A\rho} + \frac{a}{2}\dot{m}_B^3\right) \tag{A11}$$

$$\implies \frac{1}{\xi} = (aA\rho\dot{m}_B^2)\frac{\dot{m}^2}{\dot{m}_B^2} + \left(\frac{\dot{m}}{2\dot{m}_B} - \frac{3}{2}(aA\rho\dot{m}_B^2)\frac{\dot{m}}{\dot{m}_B}\right) + \left(\frac{\dot{m}_B}{2\dot{m}} + \frac{(aA\rho\dot{m}_B^2)}{2}\frac{\dot{m}_B}{\dot{m}}\right). \tag{A12}$$

Let $\hat{a} = aA\rho\dot{m}_B^2$, then

$$\frac{1}{\xi} = \hat{a}\frac{\dot{m}^2}{\dot{m}_B^2} + \left(\frac{1}{2} - \frac{3}{2}\hat{a}\right)\frac{\dot{m}}{\dot{m}_B} + \left(\frac{1}{2} + \frac{1}{2}\hat{a}\right)\frac{\dot{m}_B}{\dot{m}} \tag{A13}$$

$$\implies \frac{1}{\xi} = \frac{1}{2}\left(\frac{\dot{m}}{\dot{m}_B} + \frac{\dot{m}_B}{\dot{m}}\right) + \hat{a}\left(1 + \frac{1}{2}\frac{\dot{m}_B}{\dot{m}}\right)\left(\frac{\dot{m}}{\dot{m}_B} - 1\right)^2. \tag{A14}$$

Finally notice that

$$\frac{\dot{m}}{\dot{m}_B} = \frac{A\rho u_r}{A\rho u_r^B} = \frac{u_r}{\Omega r}\frac{\Omega r}{u_r^B} = \frac{\tan\beta_B}{\tan\beta}, \tag{A15}$$

so the stall function becomes

$$\xi = \frac{1}{\frac{1}{2}\left(\frac{\tan\beta_B}{\tan\beta} + \frac{\tan\beta}{\tan\beta_B}\right) + \hat{a}\left(1 + \frac{1}{2}\frac{\tan\beta}{\tan\beta_B}\right)\left(\frac{\tan\beta_B}{\tan\beta} - 1\right)^2}. \tag{A16}$$

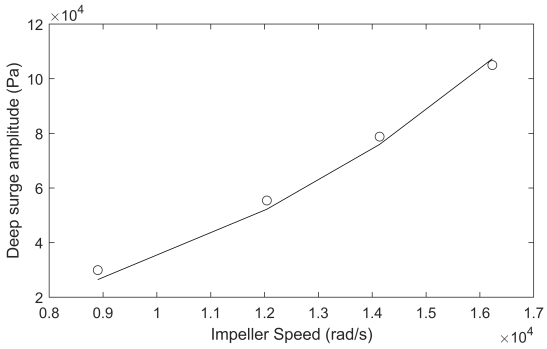

Fig. 1. Relationship between impeller speed and deep surge amplitude for stall parameter $\hat{a} = 1.7$. Test data indicated as circles has been added for comparison.

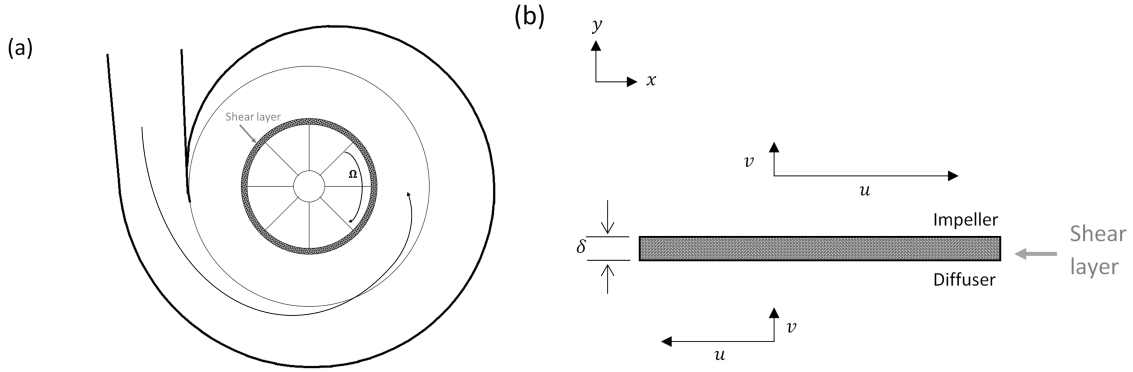

Fig. 2. Shear layer of thickness δ at the impeller-diffuser interface during reverse flow in standard geometry (a) and an x-y coordinate system (b).

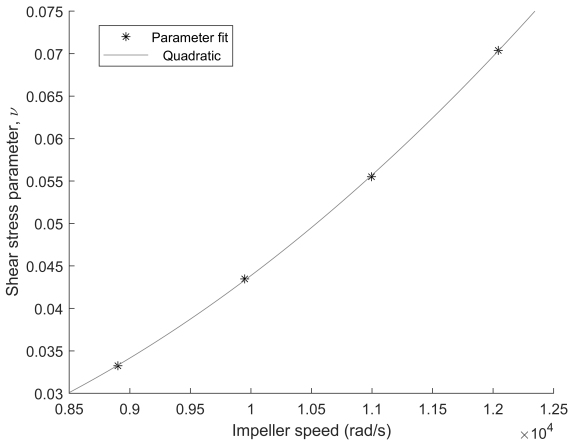

Fig. 3. Relationship for the shear loss parameter with impeller speed. The points identify the parameter value obtained where the static pressure at zero flow in the forward flow model and reverse flow model are equated.

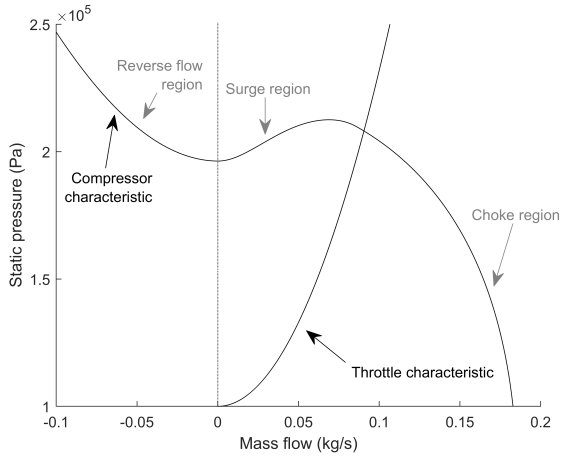

Fig. 4. Improved compressor characteristic from first principles. The throttle characteristic from Powers et al. [17] is also shown.

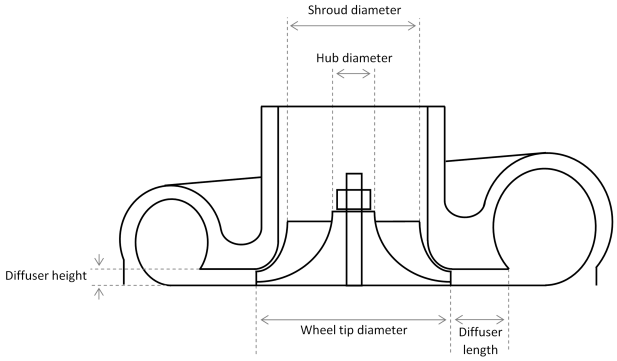

Fig. 5. Diagram indicating the dimensions given in Table 1.

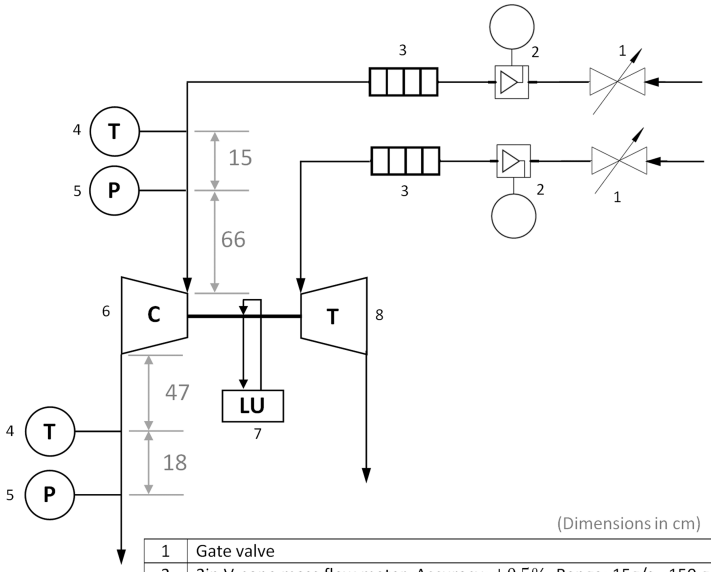

1	Gate valve
2	2in V-cone mass flow meter. Accuracy: $\pm 0.5\%$. Range: 15g/s - 150 g/s
3	Variable power electric heater
4	PRT temperature sensor. Accuracy: $\pm(0.15 + 0.002\ T)^oC$
5	Pneumatically averaged pressor sensor. Accuracy: ± 560 Pa
6	Turbocharger compressor
7	Turbocharger lubrication unit
8	Turbocharger turbine

Fig. 6. Schematic of the gas stand used for experimental testing of the compressors.

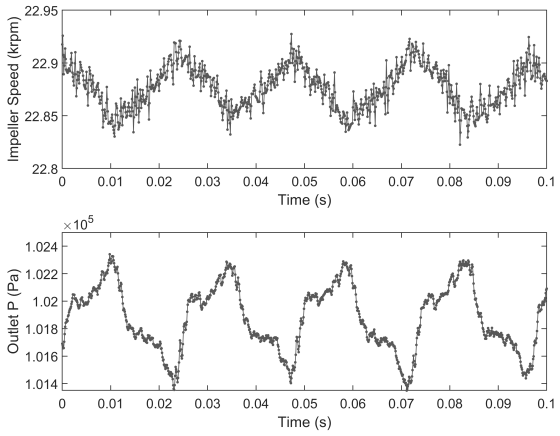

Fig. 7. Surging behaviour of the compressor when operating at zero mass flow.

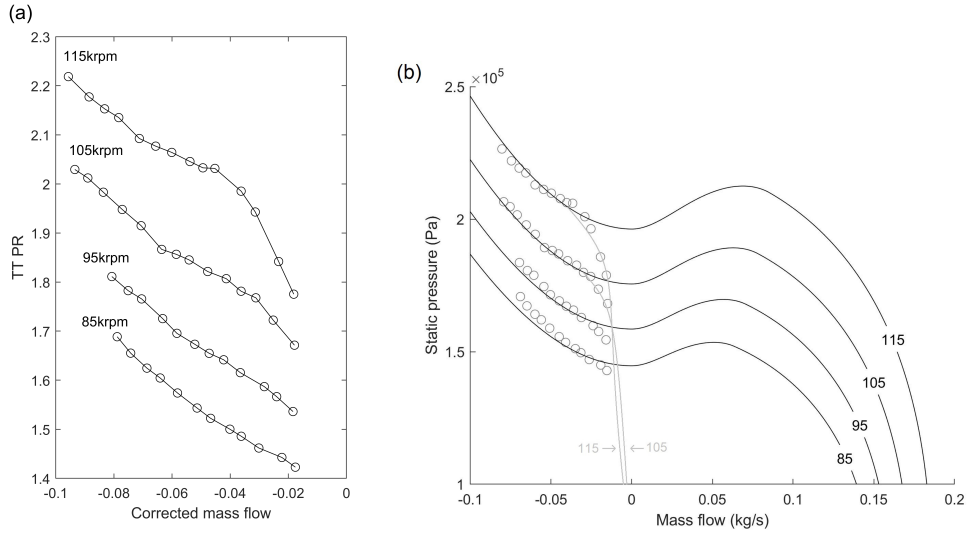

Fig. 8. Recorded compressor mappings in the negative mass flow region at different impeller speeds. (a) The raw data. (b) A comparison between the data and the model. Theoretical asymptotes for the data have been added in grey and the speeds indicated on each line are in krpm.

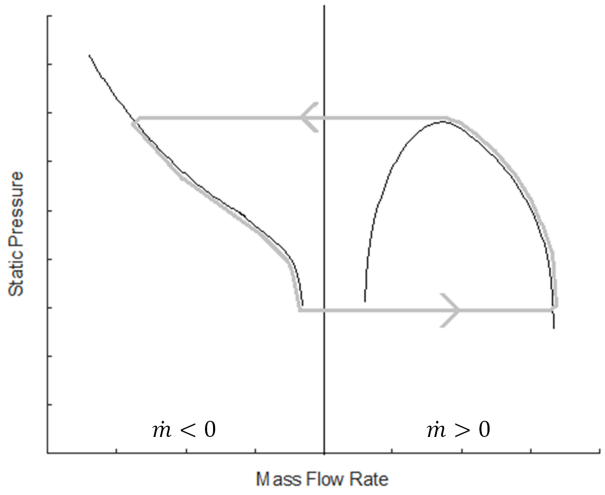

Fig. 9. Possible deep surge trajectory for high impeller speeds.

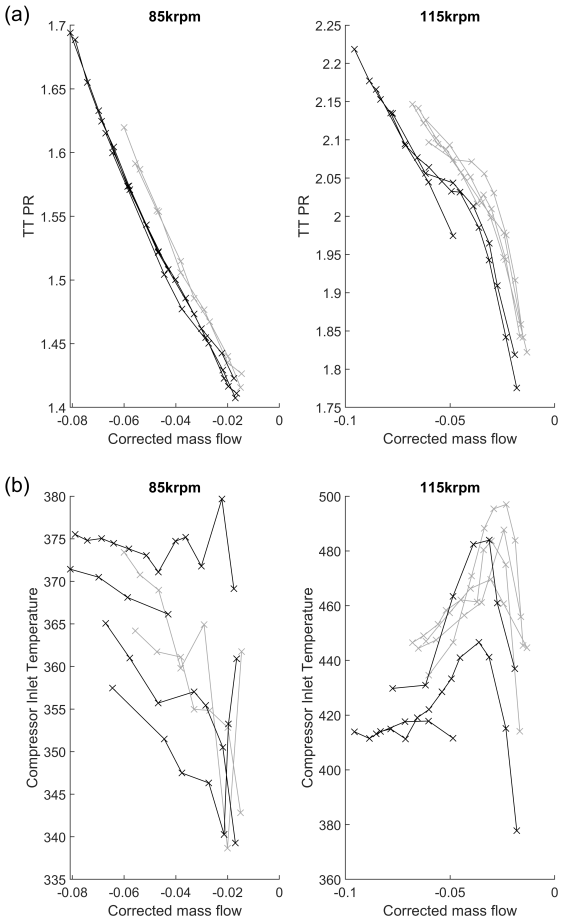

Fig. 10. (a) Repeated runs of testing for different impeller speeds. Two identical compressors were tested (one shown in grey and one in black). There are natural variations in the product which result in a shift, but the change in characteristic shape is visible in both. (b) The corresponding temperature (in K) for each test.

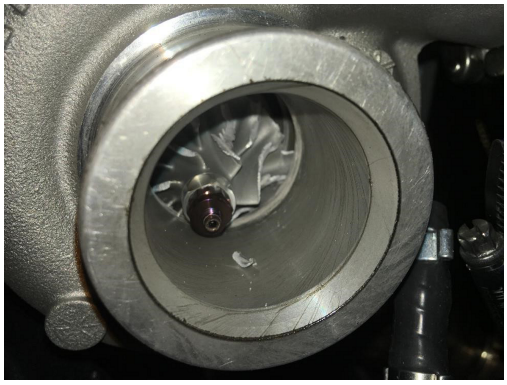

Fig. 11. Turbocharger failure as a result of testing at 135 krpm.

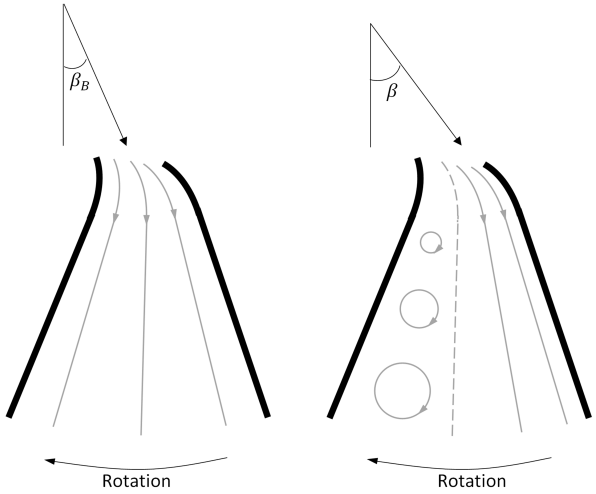

Fig. 12. Impeller channels in unstalled (left) and stalled (right) conditions.

Table 1. Geometric details of the compressor used for testing.

Number of blades	$6 + 6$
Hub diameter	13.5 mm
Shroud diameter	41 mm
Wheel tip diameter	58 mm
Diffuser height	3.15 mm
Diffuser length	16.7 mm
Diffuser area ratio	2.48
Critical area of housing	7 cm^2